Cell. Mol. Life Sci.
DOI 10.1007/s00018-013-1517-8

Cellular and Molecular Life Sciences

RESEARCH ARTICLE

The stoichiometry of peptide-heparan sulfate binding as a determinant of uptake efficiency of cell-penetrating peptides

Rike Wallbrecher · Wouter P. R. Verdurmen · Samuel Schmidt · Petra H. Bovee-Geurts · Felix Broecker · Anika Reinhardt · Toin H. van Kuppevelt · Peter H. Seeberger · Roland Brock

Received: 14 September 2013 / Revised: 18 October 2013 / Accepted: 7 November 2013
© Springer Basel 2013

Abstract Binding to negatively charged heparan sulfates (HS) at the cell surface is considered the first step in the internalization of cationic cell-penetrating peptides (CPPs). However, little is known about the relation of the characteristics of the HS-CPP interaction such as affinity, stoichiometry, and clustering with uptake. In this study, we investigated a collection of mutants of a cyclic CPP derived from human lactoferrin with respect to HS binding and uptake. The thermodynamic parameters of HS binding were determined by isothermal titration calorimetry, clustering of HS was investigated by dynamic light scattering, and cellular uptake by flow cytometry and confocal microscopy. Whereas mutations of non-arginine amino acids that are conserved across lactoferrins of different mammalia only had a minor effect on uptake efficiency, changes in the number of arginine residues influenced the uptake significantly. In general, introduction of arginine residues and cyclization improved the HS affinity and the ability to cluster HS. In particular, there was a strong negative correlation between stoichiometry and uptake, indicating that crosslinking of HS is the driving force for the uptake of arginine-rich CPPs. Using glycan microarrays presenting a collection of synthetic HS, we show that a minimal chain length of HS is required for peptide binding.

Keywords Cell-penetrating peptide (CPP) · Drug delivery · Heparan sulfate (HS) · Glycocalyx · Glycosaminoglycan

Abbreviations

CPP	Cell-penetrating peptide
DLS	Dynamic light scattering
GAG	Glycosaminoglycan
HS	Heparan sulfate
hLF	Human lactoferrin CPP
ITC	Isothermal titration calorimetry
NZ	Nucleation zones

Introduction

Cell-penetrating peptides (CPPs) are a promising class of cellular delivery vehicles for therapeutic agents such as oligonucleotides, siRNA, and proteins [1]. Structurally, CPPs are divided into multiple classes depending on their cationicity and/or amphipathicity [2]. A prominent group of the cationic CPPs are the arginine-rich peptides. In general, arginine-containing CPPs are internalized more efficiently than their lysine-containing counterparts [3]. This observation has been explained by the ability of the guanidino group to form bidentate hydrogen bonds with negatively charged heparan sulfates (HS), with acidic groups of the

Electronic supplementary material The online version of this article (doi:10.1007/s00018-013-1517-8) contains supplementary material, which is available to authorized users.

R. Wallbrecher · W. P. R. Verdurmen · S. Schmidt · P. H. Bovee-Geurts · T. H. van Kuppevelt · R. Brock (✉)
Department of Biochemistry, Nijmegen Centre for Molecular Life Sciences, Radboud University Medical Centre, Geert Grooteplein 28, 6525 GA Nijmegen, The Netherlands
e-mail: r.brock@ncmls.ru.nl

F. Broecker · A. Reinhardt · P. H. Seeberger
Department of Biomolecular Systems, Max-Planck-Institute of Colloids and Interfaces, Am Mühlenberg 1, 14476 Potsdam, Germany

F. Broecker · A. Reinhardt · P. H. Seeberger
Institute of Chemistry and Biochemistry, Freie Universität Berlin, Arnimallee 22, 14195 Berlin, Germany

Published online: 24 November 2013

lipid bilayer, and furthermore by the capacity of these complexes to partition into hydrophobic environments [4, 5].

More recently, CPPs containing one or more conformational constraints through cyclization have been an interesting addition to the field. This group of peptides includes toxin-derived peptides such as maurocalcine [6], crotamine [7], the crotamine-derived CyloP [8], as well as the CPP derived from the N-terminal antimicrobial domain of human lactoferrin, hLF [9]. For hLF and CyloP, the presence of the disulfide bridge was shown to be essential for efficient uptake. Interestingly, also for linear CPPs, cyclization has been shown to enhance uptake [10, 11].

For the hLF-derived CPP, the cyclization-dependent uptake activity was accompanied by a strong increase in the affinity for HS. HS are negatively charged, protein-linked oligosaccharides that form part of the glycocalyx [12]. For arginine-rich CPPs in more general, but also for related guanidino-rich β-peptides, binding to HS has been associated with uptake [13–16]. However, as we showed recently, the affinity of binding to HS is not a sufficient criterion for efficient uptake, as arginine-rich CPP consisting of D-amino acids internalized less effectively than their L-amino acid counterparts, despite comparable HS binding constants [17].

Several studies have described the importance of glycosaminoglycan (GAG) clustering for efficient uptake of CPPs [18–20]. Penetratin analogs with arginine residues showed stronger membrane binding than their lysine analogs, which correlated with a higher ability to cluster HS and an improved uptake [20]. Ziegler et al. [19] showed that PEGylation of the CPP WR9 that is only taken up via endocytosis and not via direct translocation in contrast to the non-PEGylated variant, did not affect HS affinity but compromised HS clustering. However, while in the cited work HS clustering was described as a factor promoting uptake, for analogs of the amphipathic CPP TP10 we showed that the size of the peptide-HS clusters could be a limiting factor for efficient uptake [21].

At present, the combination of results obtained for different peptides is a major shortcoming for generating a comprehensive picture on the involvement of HS in uptake. Here, we addressed the structure–activity relationship of HS-binding, clustering, and cellular uptake for variants of the hLF-derived CPP. We consider this CPP an ideal tool for this purpose as the requirement for a cyclic structure suggests the presence of structural determinants for efficient HS binding. Since lactoferrins are conserved across mammalia, the question arose whether conserved residues next to arginines contribute to the recognition of HS. Furthermore, by the generation of mutants that varied in the number and position of arginine residues, and in the presence and nature of the disulfide bridge the role of these structural features could be addressed without completely changing the structural context. Uptake was assessed for HS-positive cells, also after enzymatic removal of the glycocalyx, and for cells that show only little HS expression. The affinity and stoichiometry of binding to HS were determined by isothermal titration calorimetry (ITC), the capacity to cluster HS by dynamic light scattering (DLS).

The results demonstrate that cyclization primarily serves the generation of a sufficiently high local arginine density. Remarkably, for HS-positive cells, only the stoichiometry of binding showed a strong negative correlation with uptake, which indicates the requirement of HS cross-linking for inducing the uptake of arginine-containing CPPs. Consistent with this hypothesis, this correlation was not present on HS-poor cells and was abolished after enzymatic removal of the glycocalyx. Finally, to identify particular structural features relevant for the interaction of HS and the hLF CPP, we acquired interaction profiles to microarrays presenting a collection of synthetic GAGs.

Materials and methods

Cell culture

HeLa and Jurkat E6.1 leukemia cells were cultured in RPMI 1640 (Pan Biotech, Aidenbach, Germany) containing 10 % fetal calf serum (FCS). Ovcar-3 cells were cultured in RPMI containing 20 % FCS and Caco-2 cells in MEM supplemented with 20 % FCS, 1 % sodium pyruvate, and 1 % nonessential amino acids (all from Invitrogen, Eugene, USA). Cells were cultured in a humidified atmosphere, 5 % CO_2 at 37 °C and passaged every 2 or 3 days. HBS buffer pH 7.4 (10 mM HEPES, 135 mM NaCl, 5 mM KCl, 5 mM $MgCl_2$, 1.8 mM $CaCl_2$) was used for washing. All cells were originally obtained from the American Type Culture Collection (Rockville, MD, USA).

Peptides

Peptides were purchased from EMC microcollections (Tübingen, Germany). All peptides were N-terminally labeled with carboxyfluorescein and C-terminally amidated. The identity and purity of the peptides was determined by mass spectrometry and reversed-phase high-performance liquid chromatography. For formation of the intramolecular disulfide bridge, the peptides were dissolved in 50 mM HEPES buffer (pH 8) to a concentration of 1–2 mM and incubated for 2 h at 37 °C. Disulfide bridge formation was confirmed using the Ellman's test [22]. A stock solution of [5,50-dithiobis-(2-nitrobenzoic acid)] (DTNB) (Sigma Aldrich, St. Louis, MO, USA) was prepared containing 2 mM DTNB and 50 mM sodium acetate in milli-Q. For the test solution, 50 µl DTNB

solution was mixed with 100 µl of a 1 M Tris solution (pH 8), 840 µl milli-Q and 10 µl peptide solution (1–2 mM). After incubating 5 min at RT, the absorption was measured at 412 nm using a Novaspec II visible spectrophotometer (Pharmacia, New York, USA). Peptides without a disulfide bridge were dissolved in milli-Q water. Peptide concentrations were determined by measuring the absorption of fluorescein at 492 nm assuming an extinction coefficient of 75,000 $M^{-1}cm^{-1}$.

Flow cytometry

HeLa or Caco-2 cells were seeded in 24-well plates at a density of 80,000 cells (1 day) or 40,000 cells (2 days) per well prior to the experiment. 100,000 Ovcar-3 cells were seeded 1 day before the experiment. Cells were incubated with the different peptides at the indicated concentrations for 30 min at 37 °C in serum-containing medium. After washing the cells with RPMI containing 10 % FCS, cells were detached by trypsinization for 5 min at 37 °C and washed with medium by centrifugation. After resuspension, the cell-associated fluorescence was measured using a FACSCalibur flow cytometer (BD Biosciences, Erembodegem, Belgium). Analysis of 10,000 gated cells was performed using the Summit software 4.3 (Dako, Fort Collins, USA). For Jurkat E6.1 cells, a similar protocol was used with 300,000 cells per sample in a total volume of 200 µl, also including a trypsin wash step to remove membrane-bound peptides.

Confocal laser scanning microscopy

HeLa cells were seeded in chambered coverslips (Nunc, Wiesbaden, Germany) at a density of 40,000 cells (1 day) or 20,000 cells (2 days) prior to the experiment. Cells were incubated with peptides at the indicated concentrations in RPMI supplemented with 10 % FCS for 30 min and washed with RPMI containing 10 % FCS. For Jurkat cells, a cell suspension containing 300,000 cells was mixed with the peptide solution in a final volume of 200 µl and washed by centrifugation. Confocal laser scanning microscopy was performed on a TCS SP5 confocal microscope (Leica Microsystems, Mannheim, Germany) equipped with an HCX PL APO 63 × 1.2 water immersion lens. The 488-nm line of the argon ion laser was used for excitation of fluorescein and emission was collected between 500 and 550 nm.

Isothermal titration calorimetry

Peptide and HS (average molecular weight 13.6 kDa, Celsus, Cincinnati, OH, USA) solutions were diluted with HBS to yield physiological salt concentrations. ITC experiments were performed with an ITC200 Microcal (Microcal, Northampton, USA) at 25 °C. After washing the measurement cell with the peptide to coat the walls of the cell, 38 times 1 µl HS were injected into the peptide solution (220 µl). Peptide (20–60 µM) and HS (40–90 µM) concentrations were adapted for the different hLF variants in order to ensure a high signal-to-noise ratio. To correct for background heat changes, the heat changes of the five last injections which were assumed to represent exclusively dilution effects were averaged. Data were analyzed using the ITC200 Microcal software employing a one-site binding model.

Dynamic light scattering

DLS experiments were performed on a Zetasizer Nano S (Malvern Instruments, Malvern, UK) with a He–Ne laser (633 nm) and an avalanche photodiode detector at an angle of 173°. Two microliters of the different peptide solutions (50 µM) were titrated into 100 µl of a 10 µM HS solution in a ZEN0040 disposable cuvette. After mixing the sample, incubation for 3 min at 37 °C, and an additional mixing step, 3 × 12 measurements were performed. HS and peptide solutions were diluted using filtered HBS. The attenuator was set at 8 for all measurements.

Removal of the glycocalyx

Prior to peptide incubation, HS only, or the complete set of GAGs, including HS, chondroitin sulfate (CS), dermatan sulfate (DS), and hyaluronic acid (HA), and additionally the glycoprotein glycan sialic acid (SA) were removed by incubating cells for 1.5 h at 37 °C with RPMI + 1 % FCS containing 10 mU/ml heparinase III (Seikagaku, Tokyo, Japan) alone or in a cocktail with 275–550 U/ml hyaluronidase (Sigma Aldrich, St. Louis, MO, USA), 100 mU/ml chondroitinase ABC (Sigma Aldrich) and 100 mU/ml sialidase (Sigma Aldrich). After the incubation, cells were washed twice with PBS and the peptide incubation was started.

Microarray binding studies

Glycan microarrays containing synthetic HS/heparin oligosaccharides and 5-kDa natural heparin were prepared from *N*-hydroxy-succinimidyl ester-activated CodeLink slides as described previously [23–26]. After spotting of glycans, the slides were incubated overnight in a humid chamber, then quenched at 50 °C for 1 h in 50 mM aminoethanol solution, pH 9, and blocked at room temperature for 1 h with 1 % (w/v) BSA in 6 mM HEPES, pH 7.4. Slides were then washed three times with 6 mM HEPES, pH 7.4 and dried by centrifugation (5 min, 200 × *g*). For acquisition of peptide-binding profiles, slides were incubated at 4 °C

overnight with 10 μg/ml of fluorescent peptides (hLF WT: 3.25 μM, hLF Hcy: 3.22 μM, hLF +4R: 3.07 μM) in 1 % (w/v) BSA in 6 mM HEPES, pH 7.4 with 0.01 % (v/v) Tween-20 in a humid chamber. Then, slides were washed three times with 6 mM HEPES, pH 7.4 with 0.1 % (v/v) Tween-20, rinsed once with water and dried by centrifugation. Slides were scanned with a GenePix 4300A microarray scanner (Molecular Devices, Sunnyvale, CA, USA). Fluorescein was excited at 488 nm and fluorescence intensities were determined with the GenePix Pro 7 software (Molecular Devices).

Results

Impact of mutations of highly conserved amino acids on uptake efficiency

So far, the investigation of structural characteristics of the CPP hLF that relate to efficient internalization had focused on the role of the disulfide bridge. Uptake strongly depends on the presence of the bridge, as does the capacity to bind to HS [9]. These observations suggested a requirement for a particular conformational arrangement of the peptide backbone and/or amino acid side chains for the interaction with HS and possibly also for the induction of uptake. In order to further define whether this was indeed the case, several mutant peptides with single and multiple amino acid exchanges were designed. In particular, we wanted to investigate whether HS binding and uptake efficiency shared the same structure–activity relationship.

In a first set of peptides, amino acid positions that are highly conserved in lactoferrins among various species were exchanged for alanine residues (hLF W5A, hLF Q6A, hLF M9A, hLF P15A) (Table 1, Supplemental Table 1). With these mutants, we wanted to learn whether the evolutionary constraint that limited the variability of these residues was associated with uptake efficiency.

For the hLF WT peptide, we previously determined that the uptake at a concentration of 5 μM depends on endocytosis, whereas the uptake at peptide concentrations higher than 20 μM also takes place via the acid sphingomyelinase-dependent induction of nucleation zones (NZ) [9, 27, 28]. These two entry mechanisms can be distinguished by confocal microscopy and by flow cytometry. In confocal microscopy, uptake via endocytosis can be identified by punctate structures, whereas uptake via NZ leads to an intense and homogenous fluorescence throughout the cytosol and nucleus. In flow cytometry, uptake via endocytosis corresponds to a symmetric peak. Entry via NZ is reflected by a tailing of the peak towards a higher intensity. The uptake efficiencies and subcellular distributions of the hLF variants were quantified by flow cytometry and visualized by confocal microscopy, respectively (Fig. 1, Supplementary Fig. S1). When exchanging highly conserved amino acids for alanine, the uptake efficiency was decreased by a maximum of 50 % compared to hLF WT, and for all peptides the reduction was more pronounced at 5 μM as compared to 20 μM (Fig. 1a–b). Exchange of tryptophan reduced uptake by about 50 % at both concentrations, whereas exchange of methionine led to a 50 % reduction at 5 μM and a slighter reduction at 20 μM. Replacement of glutamine and also proline was without significant effect. The importance of tryptophan for the uptake of hLF is not unique for hLF but is reminiscent of the importance of this residue for the uptake of other CPPs [29–31]. Overall, the data demonstrate no particular importance of the highly conserved non-arginine residues for uptake.

Table 1 Sequences of tested hLF variants

Name	Group	Sequence
hLF WT		Fluo-KCFQWQRNMRKVRGPPVSCIKR-NH_2[a]
hLF W5A	Conserved residues	Fluo-KCFQ**A**QRNMRKVRGPPVSCIKR-NH_2
hLF Q6A		Fluo-KCFQW**A**RNMRKVRGPPVSCIKR-NH_2
hLF M9A		Fluo-KCFQWQRN**A**RKVRGPPVSCIKR-NH_2
hLF P15A		Fluo-KCFQWQRNMRKVRG**A**PVSCIKR-NH_2
hLF V12R	Arginine displacement	Fluo-KCFQWQRNMRK**R**RGPPVSCIKR-NH_2
hLF R7A		Fluo-KCFQWQ**A**NMRKVRGPPVSCIKR-NH_2
hLF R13A		Fluo-KCFQWQRNMRKV**A**GPPVSCIKR-NH_2
hLF R7A/V12R		Fluo-KCFQWQ**A**NMRK**R**RGPPVSCIKR-NH_2
hLF R13A/P15R		Fluo-KCFQWQRNMRKV**A**G**R**PVSCIKR-NH_2
hLF +4R	Arginine density	Fluo-KCF**R**WQRN**R**RKVRG**R**PV**R**CIKR-NH_2
hLF lin+4R		Fluo-K**R**F**R**WQRNMRKVRG**R**PV**RS**IKR-NH_2
hLF R7		Fluo-**R**CFQWQRNMR**R**VRGPPVSCI**R**R-NH_2
hLF K7		Fluo-KCFQWQ**K**NM**K**KV**K**GPPVSCIK**K**-NH_2
hLF Hcy	Bridge structure	Fluo-K-**Hcy**-FQWQRNMRKVRGPPVS-**Hcy**-IKR-NH_2[b]

[a] Mutated residues are indicated in *bold letters*. Fluo indicates N-terminally labeled fluorescein, NH_2 amidated C-termini

[b] Hcy refers to homocysteine in which the side chain is one methylene group longer than in cysteine

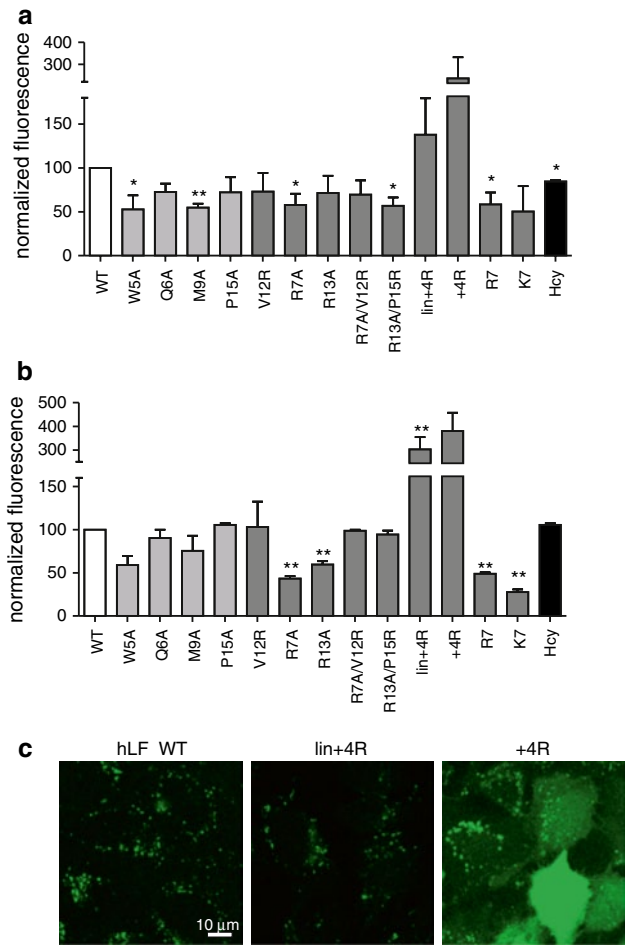

Fig. 1 Flow cytometry and confocal microscopy of hLF variants. HeLa cells were incubated with 5 µM (**a**) or 20 µM (**b**) of the indicated peptides for 30 min at 37 °C and then washed and analyzed by flow cytometry. **a**, **b** Median fluorescence of the hLF variants was normalized to hLF WT. *Bars* indicate the average of the normalized median of at least two independent experiments. *Error bars* denote the standard error of the mean (SEM). Significance of different uptake efficiencies compared to WT at $p < 0.1$ (*) or $p < 0.05$ (**) was assessed using an independent *t* test in SPSS with test-value 100 reflecting the uptake of hLF WT. **c** Confocal microscopy images after 30-min incubation with the indicated peptides (5 µM). The *scale bar* denotes 10 µm

Effects of the number and position of arginine residues and the presence and nature of the disulfide bridge

Given their prominent role in cellular delivery vectors, we designed a second set of mutants with variations in the number and position of arginine residues. In total, hLF WT contains seven positively charged residues, four of which are arginines. One of the synthetic mutants contained an additional arginine residue (hLF V12R), two variants had one arginine residue less (hLF R7A, hLF R13A), and in two mutants an arginine position was shifted (hLF R7A/V12R, hLF R13A/P15R) (Table 1). It is notable that two hLF mutants (hLF R13A and hLF R13A/P15R) were synthesized with a disrupted Cardin-Weintraub motif. This motif has been reported as a GAG binding motif [XBBXBX], with B corresponding to a basic amino acid and X corresponding to an arbitrary amino acid [32].

All modifications in which the number and/or position of the arginine residues were changed slightly decreased uptake efficiency via endocytosis (Fig. 1a, Supplementary Fig. S1, S2). However, this decreased uptake was only statistically significant for hLF R7A and hLF R13A/P15R, for which the median uptake efficiency was reduced by about 40 % at 5 µM. In contrast, for efficient internalization via NZ at 20 µM, merely a minimum number of arginine residues were required. In particular, the deletion of one arginine residue (hLF R7A, hLF R13A) significantly decreased the uptake via NZ compared to hLF WT (Fig. 1b), whereas the addition of one arginine (hLF V12R) did not improve the uptake at 20 µM. Disruption of the Cardin–Weintraub motif had little impact on uptake, which may be explained by the overall arginine content of the peptide which provides chemical groups for interaction (Fig. 1).

Previously, we had shown that a linear hLF analog without the disulfide bridge was not taken up at all nor showed binding to HS [9]. To test the hypothesis that cyclization promotes uptake by achieving an increase in local arginine density for a peptide with a rather low arginine density in the primary structure, four additional arginine residues were introduced into the linear variant (hLF lin+4R, Table 1). In addition, we also designed a cyclic counterpart with four additional arginine residues (hLF +4R). Indeed, the uptake efficiency at 5 µM of hLF lin+4R in HeLa cells was comparable to the one of hLF WT (Fig. 1a, Supplementary Fig. S1, S2), indicating that a loss of a conformation-dependent local accumulation of arginines can be compensated by an increase in arginine density in the primary peptide structure. Interestingly, at concentrations at which uptake via NZ is dominant (20 µM), the uptake of hLF lin+4R was highly improved in comparison to hLF WT (Fig. 1b). The two uptake mechanisms, endocytosis and uptake via NZ, were visible in the flow cytometry histograms, as a symmetrical peak and a shoulder, respectively (Supplementary Fig. S1). When comparing hLF lin+4R with hLF +4R that is comparing the effect of extra arginines in the absence/presence of cyclization, hLF +4R was taken up even more efficiently than hLF and hLF lin+4R at low and high concentrations (Fig. 1). These results indicate that neither hLF WT nor hLF lin+4R had incorporated the maximum capacity to trigger uptake but that only the combination of high arginine density and cyclization did. Although arginine density plays an important role in uptake via endocytosis, to our surprise, replacement of all lysines in the sequence by arginine (hLF R7, Table 1) significantly reduced the uptake efficiency at 5 and

20 μM (Fig. 1). An explanation for this finding is presented below. As expected, replacing all arginines by lysine residues (hLF K7) severely decreased the uptake even more than hLF R7 (Fig. 1).

After having shown that the uptake of the linear hLF could be restored by the introduction of arginine residues, we finally wanted to get a deeper insight into the importance of the geometry of the disulfide bridge for uptake. For this purpose, the cysteine residues were replaced by homocysteine (hLF Hcy). Homocysteine is a cysteine analog where the side chain is extended with one methylene group. At 5 μM, hLF Hcy showed a slightly reduced uptake efficiency in comparison to WT (Fig. 1a).

Dependence of uptake efficiency on HS binding

Having established a structure–activity relationship with regard to amino acid sequence and structural requirements for efficient uptake, the next step was to test whether there was a correlation between the uptake efficiencies and binding to HS chains. ITC, using soluble HS, was used for this purpose. In addition to the dissociation constant, ITC also provides information about stoichiometry, enthalpy, and entropy of binding, thereby giving a detailed view of the binding characteristics. For ITC, we focused on those arginine-rich variants that showed clear differences in the uptake efficiencies compared to hLF WT (hLF lin+4R, +4R and R7). Furthermore, we focused on hLF Hcy to obtain more insight into the role of the disulfide bridge in HS binding (Fig. 2a–e; Table 2). The two variants with four extra arginine residues had a higher affinity for HS by a factor of 2.5–5; however, there was no general correlation between the number of arginines, affinity, and internalization capacity. For example, R7 had the same affinity as hLF WT but showed a clearly decreased uptake (Fig. 2f), and even though hLF Hcy had a similar uptake efficiency as hLF WT, the K_D was clearly higher than that of hLF WT. However, a strong negative correlation was observed for the stoichiometry of binding and uptake at 5 μM (Fig. 2g). The stoichiometry varied by a factor of up to 3.5. While for hLF R7 up to 14 peptides bound per HS chain, for hLF +4R these were only 4. The fewer peptides bound per HS, the higher the uptake efficiency.

Since not only HS binding but also the ability to cluster HS had been shown to contribute to the efficiency of endocytosis of CPPs [13, 18], the capacity of the peptides to form complexes with HS was measured by DLS (Fig. 3, Supplementary Fig. S3). All peptides had the ability to cluster HS in a concentration-dependent manner except hLF K7, which did not form a significant number of clusters at all as deduced from the intensity of the scattered light (Fig. 3a). Interestingly, hLF lin+4R that showed a good uptake and had few binding sites was poor in clustering HS, whereas R7, that was poorly taken up, had the same capacity to cluster HS as hLF +4R. Clusters for all peptides had a comparable size (Fig. 3b), indicating that the scattering intensity provided valid information on the number of clusters.

Impact of glycocalyx removal on uptake efficiency

The negative correlation of uptake and stoichiometry revealed a clearly defined impact of the glycocalyx on peptide uptake. Furthermore, the differences in stoichiometry demonstrated that the peptides differed in their capacity to engage the glycocalyx. We therefore hypothesized that removal of the glycocalyx should affect peptide uptake in a non-uniform manner. Two hypotheses are conceivable: First, for peptides with a high stoichiometry, the glycocalyx may act as a buffer, leading to an enhancement of uptake upon GAG removal for those peptides in particular. Second, a low stoichiometry may promote uptake, because these peptides are efficiently cross-linking the glycocalyx. Then, removal of the glycocalyx should lead to reduced uptake of these peptides. In order to address these hypotheses, HS was removed by a heparinase treatment. Surprisingly, HS removal did not have any effect on the uptake of any of the tested peptides (Supplementary Fig. S4). We have already shown earlier that heparinase treatment greatly reduced

Table 2 Thermodynamic parameters derived from ITC binding studies between hLF variants and HS

	Arginines (*n*)	Sites per HS (*n*)	K_D (μM)	Enthalpy ($kcal^{-1}$ mol^{-1})	Entropy (cal^{-1} mol^{-1} deg^{-1})	Enthalpy (per hLF)	Enthalpy (per Arg)
hLF WT_3[a]	4	9 ± 1[b]	0.64 ± 0.07	−31 ± 5	−75 ± 15	−3 ± 1	−0.78 ± 0.22
lin+$4R_4$	8	6 ± 1	0.24 ± 0.04	−41 ± 15	−106 ± 4	−7 ± 1	−0.93 ± 0.17
$+4R_2$	8	4 ± 1	0.12 ± 0.01	−35 ± 3	−84 ± 11	−9 ± 3	−1.11 ± 0.32
$R7_3$	7	14 ± 0.4	0.53 ± 0.07	−84 ± 12	−254 ± 44	−6 ± 1	−0.88 ± 0.13
Hcy_2	4	10 ± 2	1.17 ± 0.10	−35 ± 2	−91 ± 7	−4 ± 0.4	−0.92 ± 0.10

[a] The number of measurements is indicated as a *subscript* behind the peptide name

[b] Errors denote standard deviations

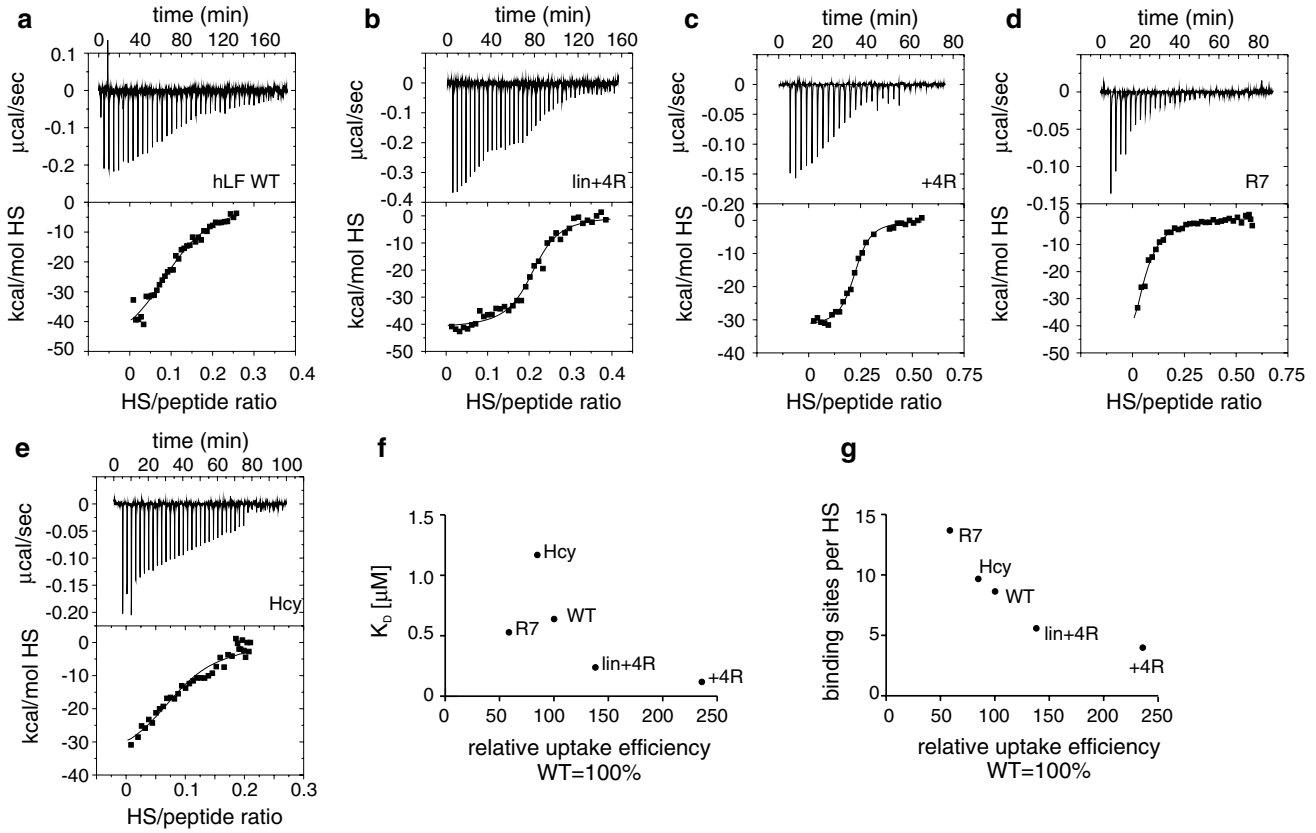

Fig. 2 ITC measurements for the interaction of hLF variants with HS. **a**–**e** *Upper panels* raw ITC data showing the heat changes over the time course of a single experiment. One peak corresponds to one injection of HS into the cell with peptide. *Lower panels* integrated heats per HS injection as a function of the molar ratio of HS/peptide. Correlations between binding constant (**f**) and stoichiometry (**g**) with the uptake efficiency at 5 µM in HeLa cells. Each *point* represents the mean of at least two experiments. *Error ranges* are shown in Table 2

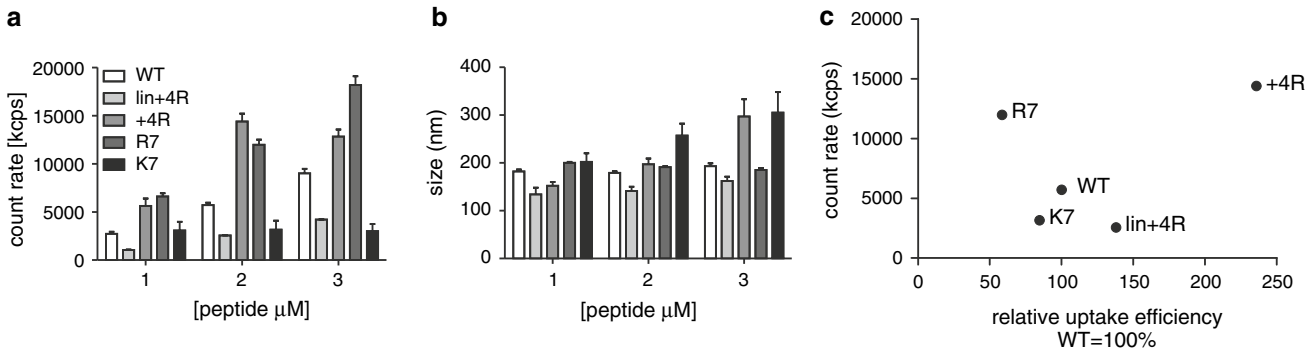

Fig. 3 Determination of complex formation by dynamic light scattering. The indicated concentrations of the peptides were titrated into 50 µM HS and the count rate and sizes of complexes were measured; **a** count rate, **b** cluster size. The capacity to cluster HS is inferred from the count rate of scattered light measured in HBS at 37 °C. *Error bars* denote standard errors of the mean of at least two independent experiments. **c** Correlation between count rate (at a peptide concentration of 2 µM) and uptake efficiency at 5 µM in HeLa cells

membrane binding of hLF but had only little effect on uptake [9]. Since the glycocalyx is not only composed of HS but also of other negatively charged sugars, such as the GAGs, CS and DS as well as HA and SA, we completely digested the glycocalyx of HeLa cells using an enzyme cocktail. The efficiency of removal of the sugars was confirmed by staining the specific epitopes with antibodies (Supplementary Fig. S5). The membrane integrity was not affected by the GAG removal, as was confirmed by the absence of an increased propidium iodide staining

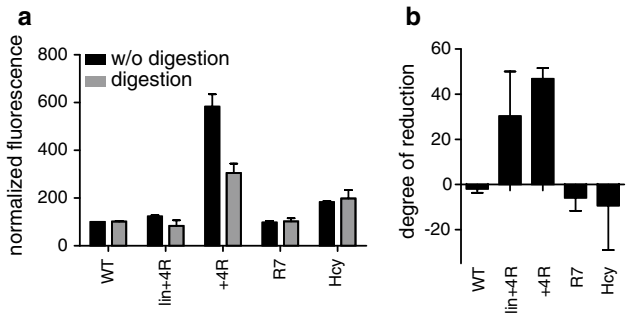

Fig. 4 Peptide uptake at 5 μM after full digestion of the glycocalyx. After removal of HS, CS, DS, HA, and SA for 1.5 h, the uptake of the indicated peptide variants was quantified by flow cytometry. **a** Comparison of fluorescence with and without digestion. **b** Degree of reduction after digestion compared to non-treated cells. *Error bars* denote SEM ($n = 2$)

in comparison to the untreated control (Supplementary Fig. S5). Complete digestion of the whole glycocalyx decreased uptake of hLF +4R and hLF lin+4R by about 50 and 30 % at 5 μM, respectively (Fig. 4, Supplementary Fig. S6). In contrast, uptake of the wild-type peptide and the R7 and Hcy variants remained unaffected, supporting an uptake-promoting role of the glycocalyx for the peptides with a low stoichiometry and refuting the hypothesis of a buffering effect.

Cell line dependence of the uptake of hLF variants

The negative correlation of stoichiometry of binding with uptake and the effect of GAG removal indicated that efficient cross-linking of HS chains promotes rather than compromises uptake. In order to exclude that this correlation is a particular characteristic of HeLa cells, we compared uptake in HeLa cells with two cells lines positive for HS (Caco-2 [33, 34] and Ovcar-3 cells [35, 36]). In addition, we also included Jurkat cells in our analysis as this cell line carries only a few GAGs [17, 21]. For these cells, uptake efficiency should be independent of stoichiometry, similar to HeLa cells after enzymatic GAG removal. Because Jurkat cells are more sensitive to peptide uptake both in the induction of NZ-dependent uptake and toxicity, peptide concentrations were adjusted to 1 and 5 μM. The relative uptake efficiencies in the HS-expressing cell lines Caco-2 and Ovcar-3 were very similar to the ones of HeLa cells (Supplementary Fig. S9). Primarily, for all GAG-positive cells, the +4R variants showed a strongly increased uptake in comparison to the other variants and the uptake of R7 and K7 was lower than the one of the hLF WT peptide.

In contrast, in Jurkat cells, the uptake of hLF lin+4R and hLF +4R relative to hLF WT was decreased at low concentrations (1 μM), whereas the uptake of hLF R7 and hLF K7 was reduced to a much smaller extent compared to

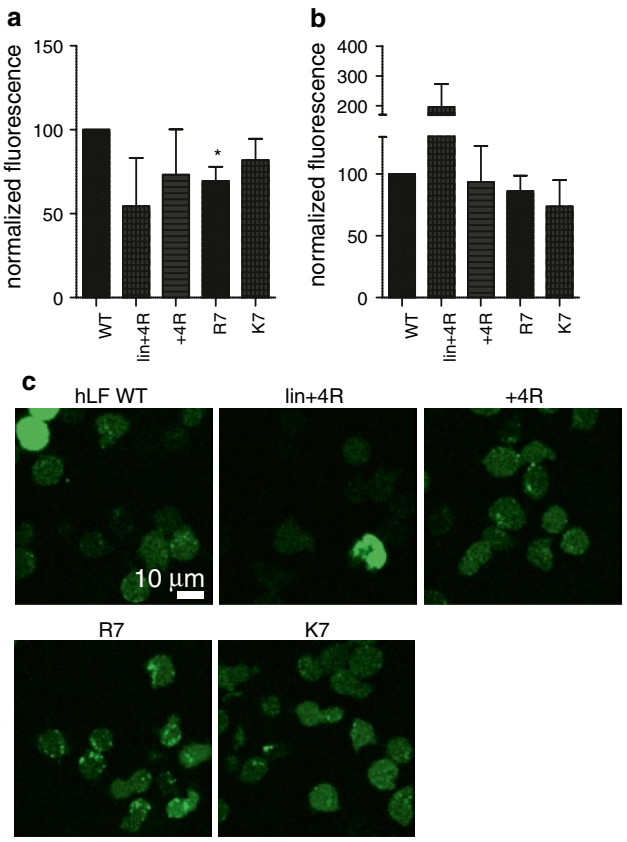

Fig. 5 Uptake of hLF variants in Jurkat cells. Jurkat cells were incubated with 1 μM (**a**) or 5 μM (**b**) of the indicated peptides for 30 min at 37 °C, washed and analyzed by flow cytometry. **a**, **b** Median fluorescence of the hLF variants was normalized to hLF WT. *Bars* indicate the average of the median of at least three independent experiments. *Error bars* denote the standard error of the mean (SEM). **c** Confocal microscopy images of 1 μM of the peptides incubated for 30 min at 37 °C

HeLa cells (Fig. 5, Supplemental Fig. S7, S8). Therefore, consistent with our hypothesis, for Jurkat cells the relative uptake efficiencies were more similar to the GAG-digested HeLa cells than to the untreated HeLa cells. At 5 μM, the uptake pattern was more similar to that in HeLa cells except that the uptake of hLF +4R was as efficient as hLF WT, consistent with the fact that at this higher concentration endocytosis-independent uptake via NZ is triggered.

Definition of structural determinants in HS binding

After the determination of the HS binding characteristics by ITC and DLS, two broadly used techniques to characterize HS binding in the field of CPPs, we wanted to take the analysis of the peptide-HS interaction a step further and determine whether there are structural determinants of HS itself that lead to binding preferences for all or individual peptides. For this purpose, the HS binding of hLF WT, hLF

Hcy and hLF +4R which differ in uptake efficiency and stoichiometry was measured using microarrays carrying a collection of synthetic glycans of various length and degree of sulfation (Fig. 6a) [23–26]. All peptides bound to 5-kDa natural heparin (Fig. 6b–d). When comparing the intensities of the signals, the binding patterns for the three hLF variants showed clearly distinct binding profiles. hLF WT and hLF Hcy bound to all structures. The binding of hLF Hcy was weaker than that of hLF WT which is in agreement with the lower binding affinity for HS compared to hLF WT (Table 2). To our surprise, hLF +4R could only be detected on structures **5** and **9** at very low intensities and on the control 5-kDa heparin in spite of its high affinity for HS. For the other signals, no clear correlation could be found between structural characteristics and binding intensities except that structures with *N*-sulfation showed stronger binding than the *N*-acetylated variants (e.g., structure **3** vs. **4**). In addition, whereas 2-*O*-sulfation promotes binding (e.g., structure **6**), 6-*O*-sulfation is disadvantageous (e.g., structure **2** vs. **6**). Very clearly, charge alone is insufficient to explain binding preferences.

Discussion

Binding of CPPs to HS has been described to support efficient internalization via endocytosis [13–16]. However, there is still no consistent picture on the relationships of HS binding and CPP internalization. In order to gain more insight into the interdependence of the HS interaction and internalization, we designed a set of hLF derivatives varying in the number and position of arginine residues.

Using ITC for a subset of variants, we obtained a comprehensive analysis of the thermodynamics and stoichiometry of HS binding. Very interestingly, even though binding constants differed by up to one order of magnitude, there was no clear correlation of affinity for HS and uptake. This finding is in line with our previous results for L-peptides and their D-counterpart [17] which, in spite of identical affinities, showed a strongly reduced uptake of the D-peptides, indicative of a chirality-sensitive trigger. Here, we found, in addition to the chirality-sensitive trigger, a strong negative correlation between the stoichiometry of HS binding and endocytic uptake (Fig. 2). We considered two different hypotheses as the basis for this observation. First, the glycocalyx could act as a buffer, sequestering those peptides with a high stoichiometry and thus reducing their uptake. Second, peptides with a low stoichiometry could have a stronger capacity to cross-link HS thus leading to efficient internalization (Fig. 7). The fact that removal of the glycocalyx reduced the uptake of the low stoichiometry peptides while not affecting the uptake of the high stoichiometry peptides strongly favors the second hypothesis. Cross-linking of the glycocalyx by hLF lin+4R and hLF +4R contributes to the high uptake of these peptides, while contributing less to the uptake of hLF R7. This model is also supported by the similarity of uptake profiles for HS-positive cells and the reduced uptake of hLF lin+4R and hLF +4R in HS-poor Jurkat cells. Neither for GAG-digested HeLa cells nor for Jurkat cells was a correlation between uptake and stoichiometry present (Supplementary Fig. S10). It will be interesting to explore to which extent this correlation also holds for D-peptides, which showed a reduced capacity to induce endocytosis. Such experiments should answer the question whether GAG cross-linking and the elusive chirality-dependent trigger are part of the same molecular mechanism.

Remarkably, the capacity to cluster HS, as measured by DLS, did neither correlate with the binding stoichiometry nor with uptake efficiency. This observation adds a shade to the more general concept that associates the capacity to cluster HS to uptake [18], a concept that is also violated for variants of the CPP TP10 [21]. Very clearly, cross-linking of HS on the cell surface depends to a larger extent on the stoichiometry of binding than clustering in solution.

Interestingly, Ziegler and Seelig showed that the CPP WR_9 that was able to induce GAG clustering showed uptake via endocytosis and NZ, while a PEGylated variant that failed to cluster GAG was taken up by endocytosis only [19]. These results are in agreement with our findings that hLF +4R being the most efficient in clustering HS, was also the only peptide showing uptake via NZ at 5 μM (Fig. 1). However, our data also supports a positive effect of GAG clustering on induction of endocytosis, which was also shown for other guanidinium-rich transporters and polyplexes [37, 38]. As an alternative explanation for an induction of NZ-dependent uptake via HS clustering, it may be possible that when fewer peptide molecules are sequestered by HS, a higher amount of peptide is still available that may be taken up via NZ.

Despite the strong negative correlation of stoichiometry and uptake, we did not arrive at a consistent structural model to explain the differences in stoichiometry. Of those peptides that showed good uptake efficiencies and contained more arginine residues (e.g., lin+4R, +4R) fewer peptide molecules were bound to one HS molecule (Table 2), consistent with charge neutralization as the underlying principle [18, 39]. Remarkably, hLF +4R, having the best capability of clustering HS, showed a binding stoichiometry that was the closest to charge neutralization compared to the other peptides tested. This estimate is based on the sulfur content of 5.4 % of the HS used in ITC, which can be translated into 23 sulfonic acid groups. These sulfonic acid groups are co-occurring with ~23 carboxyl groups leading to 46 charges in total and as hLF +4R has 11 positive charges and four hLF +4R are binding per HS,

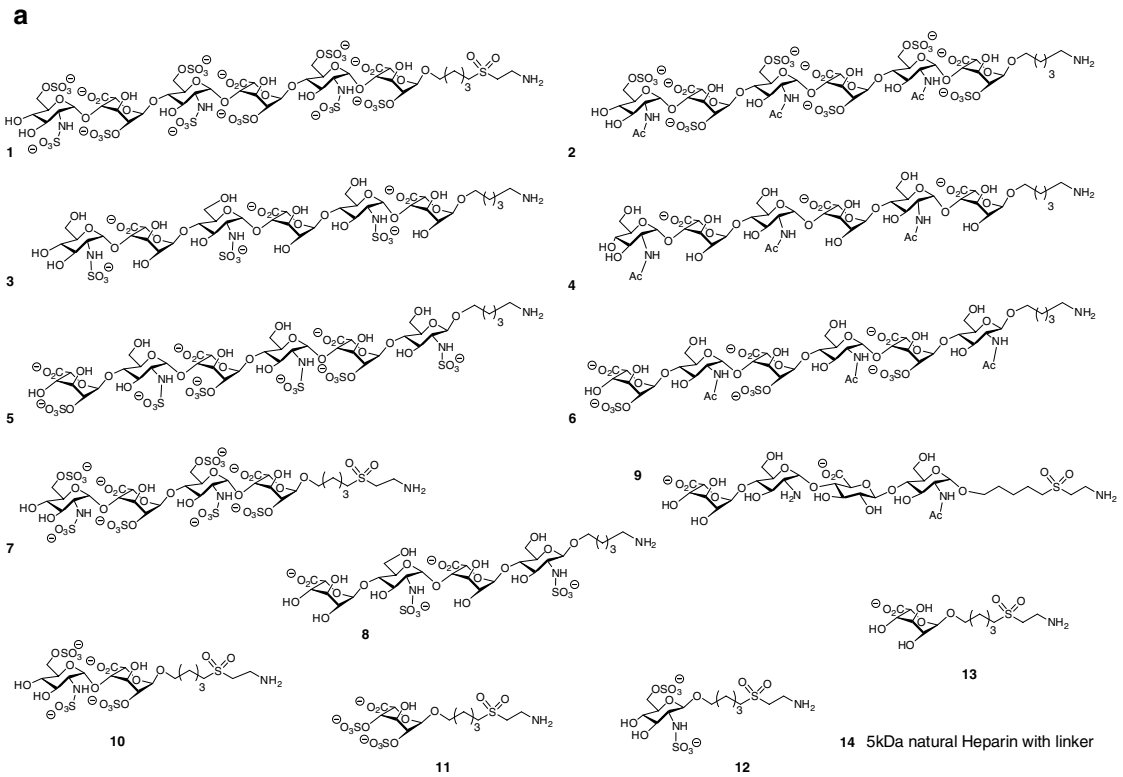
a
1
2
3
4
5
6
7
8
9
10
11
12
14 5kDa natural Heparin with linker

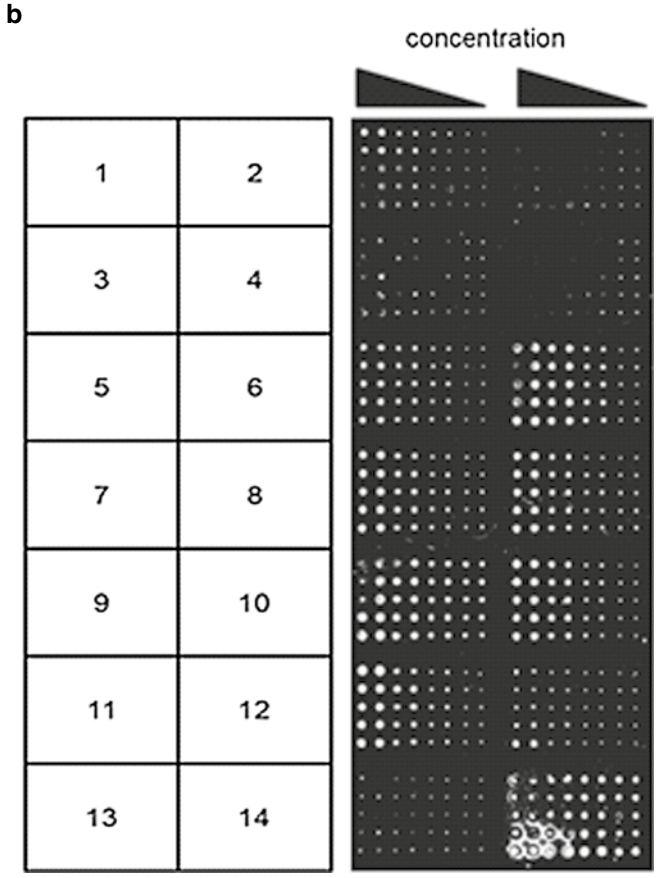
b
concentration
1
2
3
4
5
6
7
8
9
10
11
12
13
14

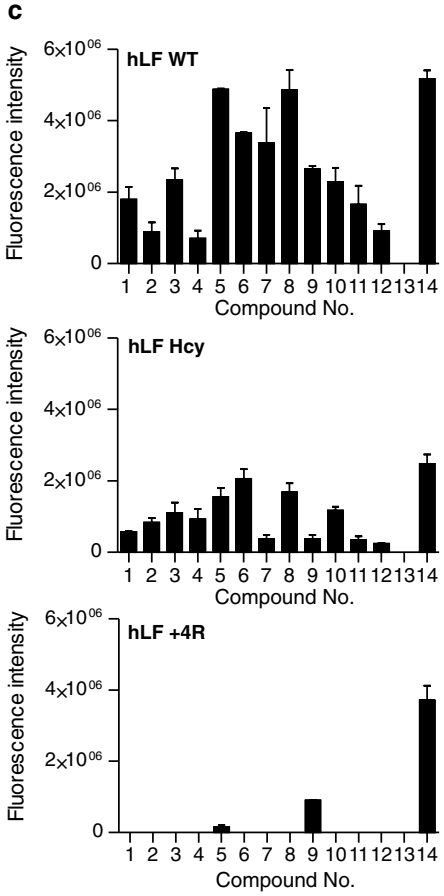
c
hLF WT
hLF Hcy
hLF +4R
Fluorescence intensity
Compound No.
6x10^06
4x10^06
2x10^06
0
1 2 3 4 5 6 7 8 9 10 11 12 13 14

◀ **Fig. 6** Binding of hLF variants to glycan microarrays. **a** Molecular structures, **b** microarray layout and peptide binding shown for hLF WT, **c** binding specificities of the three tested peptides. Fluorescence intensity values (excitation wavelength 488 nm) were determined using the GenePix Pro 7 software (Molecular Devices). Mean values ± SEM of $n = 20$ spots at the highest concentrations of two independent microarrays are plotted

roughly all charges are neutralized. However, the importance of arginine residues for binding HS and the occurrence of charge neutralization was violated by hLF R7 for which replacement of all lysine residues by arginines resulted in a much higher stoichiometry and also had a negative impact on the uptake efficiency.

Using microarrays carrying HS structures with different length and degree of sulfation, most strikingly, hLF +4R that had the lowest binding stoichiometry showed the poorest interaction with the microarrays. This observation can be explained by the fact that the synthetic oligosaccharides were too short to provide binding sites for all arginine residues in the peptide. Consistent with this consideration, with a molecular weight of the HS used in ITC of 13.63 kDa and on average 55 sugars per chain, hLF WT and hLF Hcy engage six sugar units, which matches the lengths of the strongly bound HS on the microarrays. The lower binding affinities for hLF Hcy compared to hLF WT can be explained by the lower binding affinity measured by ITC. In contrast, hLF +4R requires nine sugar molecules (2.3 kDa) for binding which on the array was only provided by the natural 15-kDa heparin. It is important to note that in nature, the HS chain length is much longer than the synthetic HS structures: HS vary between 5 and 70 kDa corresponding to 15–230 times larger than the HS structures on the microarray [40].

When testing the biological effect of HS removal on HeLa cells, only a weak and poorly reproducible reduction of uptake was observed. However, when the whole glycocalyx including CS, DS, and also HA and SA were removed, a strong reduction in uptake was observed for hLF +4R (Fig. 4) being most efficient in clustering HS. These results indicate that not only HS are involved in the uptake of arginine-rich CPP but also the other sugars of the glycocalyx. So far, the focus on GAG involvement for CPP uptake has mostly been on HS. Recently, the involvement of SA and other GAGs was studied for CPP but a clear picture about the structural requirements for efficient CPP binding and internalization is still missing and should be investigated in more detail [41, 42].

In conclusion, by performing a detailed analysis of uptake, binding constants and stoichiometry for a set of variants of the lactoferrin-derived CPP, we established a well-defined structure–activity relationship for HS binding and uptake where stoichiometry was the decisive factor. This finding sheds more light on the mechanism of uptake of arginine-rich CPP but more importantly, indicates that in the further development of CPP, even with the same number of positively charged residues, well-defined functional characteristics exist that control uptake activity. We expect our observations to hold for other members of the class of arginine-rich peptides. Even though not addressed yet, it is reasonable to speculate that stoichiometry may also

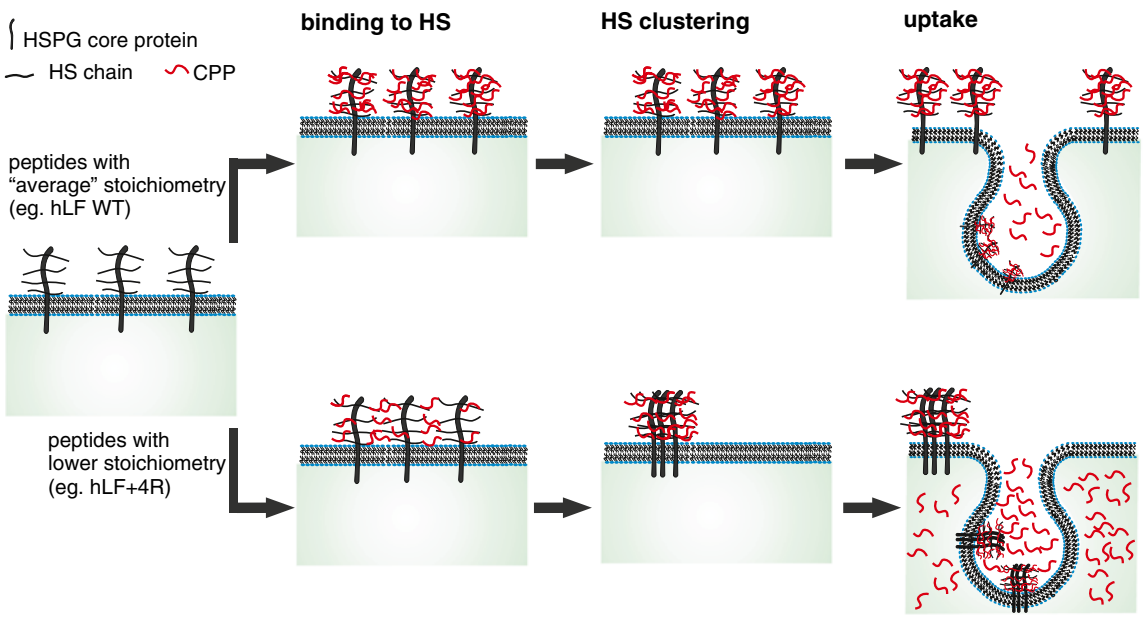

Fig. 7 Schematic of the proposed stoichiometry-dependence of uptake. With a higher binding stoichiometry, peptides have a limited capacity to cross-link HS. In contrast, peptides with a low stoichiometry effectively cross-link HS, leading to proteoglycan clustering and internalization

contribute to the dependence of uptake on peptide length for oligoarginines [43]. Nevertheless, we have already shown before that this observation does not hold for other classes of CPP [21]. Such knowledge may be decisive when considering future in vivo applications to avoid sequestration in the glycocalyx, but instead achieve efficient cellular delivery.

Acknowledgments We would like to thank the Max Planck Society and the Studienstiftung des Deutschen Volkes for their generous support of this work (scholarship to AR).

References

1. Andaloussi SE, Lehto T, Lundin P, Langel U (2011) Application of PepFect peptides for the delivery of splice-correcting oligonucleotides. Methods Mol Biol 683:361–373. doi:10.1007/978-1-60761-919-2_26
2. Milletti F (2012) Cell-penetrating peptides: classes, origin, and current landscape. Drug Discov Today. doi:10.1016/j.drudis.2012.03.002
3. Futaki S, Goto S, Sugiura Y (2003) Membrane permeability commonly shared among arginine-rich peptides. J Mol Recognit 16(5):260–264
4. Rothbard JB, Jessop TC, Wender PA (2005) Adaptive translocation: the role of hydrogen bonding and membrane potential in the uptake of guanidinium-rich transporters into cells. Adv Drug Deliv Rev 57(4):495–504
5. Sakai N, Matile S (2003) Anion-mediated transfer of polyarginine across liquid and bilayer membranes. J Am Chem Soc 125(47):14348–14356
6. Esteve E, Mabrouk K, Dupuis A, Smida-Rezgui S, Altafaj X, Grunwald D, Platel JC, Andreotti N, Marty I, Sabatier JM, Ronjat M, De Waard M (2005) Transduction of the scorpion toxin maurocalcine into cells. Evidence that the toxin crosses the plasma membrane. J Biol Chem 280(13):12833–12839. doi:10.1074/jbc.M412521200
7. Kerkis A, Kerkis I, Radis-Baptista G, Oliveira EB, Vianna-Morgante AM, Pereira LV, Yamane T (2004) Crotamine is a novel cell-penetrating protein from the venom of rattlesnake *Crotalus durissus terrificus*. Faseb J 18(12):1407–1409. doi:10.1096/fj.03-1459fje
8. Jha D, Mishra R, Gottschalk S, Wiesmuller KH, Ugurbil K, Maier ME, Engelmann J (2011) CyLoP-1: a novel cysteine-rich cell-penetrating peptide for cytosolic delivery of cargoes. Bioconjug Chem 22(3):319–328. doi:10.1021/bc100045s
9. Duchardt F, Ruttekolk IR, Verdurmen WP, Lortat-Jacob H, Burck J, Hufnagel H, Fischer R, van den Heuvel M, Lowik DW, Vuister GW, Ulrich A, de Waard M, Brock R (2009) A cell-penetrating peptide derived from human lactoferrin with conformation-dependent uptake efficiency. J Biol Chem 284(52):36099–36108
10. Aubry S, Burlina F, Dupont E, Delaroche D, Joliot A, Lavielle S, Chassaing G, Sagan S (2009) Cell-surface thiols affect cell entry of disulfide-conjugated peptides. Faseb J 23(9):2956–2967. doi:10.1096/Fj.08-127563
11. Lattig-Tunnemann G, Prinz M, Hoffmann D, Behlke J, Palm-Apergi C, Morano I, Herce HD, Cardoso MC (2011) Backbone rigidity and static presentation of guanidinium groups increases cellular uptake of arginine-rich cell-penetrating peptides. Nat Commun 2:453. doi:10.1038/ncomms1459
12. Bernfield M, Gotte M, Park PW, Reizes O, Fitzgerald ML, Lincecum J, Zako M (1999) Functions of cell surface heparan sulfate proteoglycans. Annu Rev Biochem 68:729–777. doi:10.1146/annurev.biochem.68.1.729
13. Goncalves E, Kitas E, Seelig J (2005) Binding of oligoarginine to membrane lipids and heparan sulfate: structural and thermodynamic characterization of a cell-penetrating peptide. Biochemistry 44(7):2692–2702
14. Tyagi M, Rusnati M, Presta M, Giacca M (2001) Internalization of HIV-1 tat requires cell surface heparan sulfate proteoglycans. J Biol Chem 276(5):3254–3261
15. Poon GM, Gariepy J (2007) Cell-surface proteoglycans as molecular portals for cationic peptide and polymer entry into cells. Biochem Soc Trans 35(Pt 4):788–793
16. Ram N, Aroui S, Jaumain E, Bichraoui H, Mabrouk K, Ronjat M, Lortat-Jacob H, de Waard M (2008) Direct peptide interaction with surface glycosaminoglycans contributes to the cell penetration of maurocalcine. J Biol Chem 283(35):24274–24284
17. Verdurmen WP, Bovee-Geurts PH, Wadhwani P, Ulrich AS, Hallbrink M, van Kuppevelt TH, Brock R (2011) Preferential uptake of L-versus D-amino acid cell-penetrating peptides in a cell type-dependent manner. Chem Biol 18(8):1000–1010. doi:10.1016/j.chembiol.2011.06.006
18. Ziegler A, Seelig J (2008) Binding and clustering of glycosaminoglycans: a common property of mono- and multivalent cell-penetrating compounds. Biophys J 94(6):2142–2149
19. Ziegler A, Seelig J (2011) Contributions of glycosaminoglycan binding and clustering to the biological uptake of the nonamphipathic cell-penetrating peptide WR9. Biochemistry 50(21):4650–4664. doi:10.1021/bi1019429
20. Amand HL, Rydberg HA, Fornander LH, Lincoln P, Norden B, Esbjorner EK (2012) Cell surface binding and uptake of arginine- and lysine-rich penetratin peptides in absence and presence of proteoglycans. Biochim Biophys Acta 1818(11):2669–2678. doi:10.1016/j.bbamem.2012.06.006
21. Verdurmen WP, Wallbrecher R, Schmidt S, Eilander J, Bovee-Geurts P, Fanghanel S, Burck J, Wadhwani P, Ulrich AS, Brock R (2013) Cell surface clustering of heparan sulfate proteoglycans by amphipathic cell-penetrating peptides does not contribute to uptake. J Control Release 170(1):83–91. doi:10.1016/j.jconrel.2013.05.001
22. Ellman GL (1959) Tissue sulfhydryl groups. Arch Biochem Biophys 82(1):70–77
23. Adibekian A, Bindschadler P, Timmer MS, Noti C, Schutzenmeister N, Seeberger PH (2007) De novo synthesis of uronic acid building blocks for assembly of heparin oligosaccharides. Chemistry 13(16):4510–4522. doi:10.1002/chem.200700141
24. de Paz JL, Noti C, Seeberger PH (2006) Microarrays of synthetic heparin oligosaccharides. J Am Chem Soc 128(9):2766–2767. doi:10.1021/ja057584v
25. Hecht ML, Rosental B, Horlacher T, Hershkovitz O, De Paz JL, Noti C, Schauer S, Porgador A, Seeberger PH (2009) Natural cytotoxicity receptors NKp30, NKp44 and NKp46 bind to different heparan sulfate/heparin sequences. J Proteome Res 8(2):712–720. doi:10.1021/pr800747c
26. Noti C, de Paz JL, Polito L, Seeberger PH (2006) Preparation and use of microarrays containing synthetic heparin oligosaccharides for the rapid analysis of heparin–protein interactions. Chemistry 12(34):8664–8686. doi:10.1002/chem.200601103
27. Duchardt F, Fotin-Mleczek M, Schwarz H, Fischer R, Brock R (2007) A comprehensive model for the cellular uptake of cationic cell-penetrating peptides. Traffic 8(7):848–866. doi:10.1111/j.1600-0854.2007.00572.x
28. Verdurmen WP, Thanos M, Ruttekolk IR, Gulbins E, Brock R (2010) Cationic cell-penetrating peptides induce ceramide formation via acid sphingomyelinase: implications for uptake. J Control Release 147(2):171–179. doi:10.1016/j.jconrel.2010.06.030
29. Dom G, Shaw-Jackson C, Matis C, Bouffioux O, Picard JJ, Prochiantz A, Mingeot-Leclercq MP, Brasseur R, Rezsohazy R

(2003) Cellular uptake of Antennapedia Penetratin peptides is a two-step process in which phase transfer precedes a tryptophan-dependent translocation. Nucleic Acids Res 31(2):556–561
30. Lecorche P, Walrant A, Burlina F, Dutot L, Sagan S, Mallet JM, Desbat B, Chassaing G, Alves ID, Lavielle S (2011) Cellular uptake and biophysical properties of galactose and/or tryptophan containing cell-penetrating peptides. Biochim Biophys Acta. doi:10.1016/j.bbamem.2011.12.003
31. Derossi D, Joliot AH, Chassaing G, Prochiantz A (1994) The third helix of the Antennapedia homeodomain translocates through biological membranes. J Biol Chem 269(14):10444–10450
32. Cardin AD, Weintraub HJ (1989) Molecular modeling of protein-glycosaminoglycan interactions. Arteriosclerosis 9(1):21–32
33. Levy P, Robert A, Picard J (1988) Biosynthesis of glycosaminoglycans in the human colonic tumor cell line Caco-2: structural changes occurring with the morphological differentiation of the cells. Biol Cell 62(3):255–264
34. Molist A, Romaris M, Lindahl U, Villena J, Touab M, Bassols A (1998) Changes in glycosaminoglycan structure and composition of the main heparan sulphate proteoglycan from human colon carcinoma cells (perlecan) during cell differentiation. Eu J Biochem 254(2):371–377
35. Fretz MM, Koning GA, Mastrobattista E, Jiskoot W, Storm G (2004) OVCAR-3 cells internalize TAT-peptide modified liposomes by endocytosis. Biochim Biophys Acta 1665(1–2):48–56. doi:10.1016/j.bbamem.2004.06.022
36. Kokenyesi R (2001) Ovarian carcinoma cells synthesize both chondroitin sulfate and heparan sulfate cell surface proteoglycans that mediate cell adhesion to interstitial matrix. J Cell Biochem 83(2):259–270
37. Inoue M, Tong W, Esko JD, Tor Y (2013) Aggregation-mediated macromolecular uptake by a molecular transporter. ACS Chem Biol. doi:10.1021/cb400172h
38. Rehman Z, Sjollema KA, Kuipers J, Hoekstra D, Zuhorn IS (2012) Nonviral gene delivery vectors use syndecan-dependent transport mechanisms in filopodia to reach the cell surface. ACS Nano 6(8):7521–7532. doi:10.1021/nn3028562
39. Ziegler A, Seelig J (2004) Interaction of the protein transduction domain of HIV-1 TAT with heparan sulfate: binding mechanism and thermodynamic parameters. Biophys J 86(1 Pt 1):254–263
40. Iozzo RV (2001) Heparan sulfate proteoglycans: intricate molecules with intriguing functions. J Clin Investig 108(2):165–167. doi:10.1172/JCI13560
41. Alves ID, Bechara C, Walrant A, Zaltsman Y, Jiao CY, Sagan S (2011) Relationships between membrane binding, affinity and cell internalization efficacy of a cell-penetrating peptide: penetratin as a case study. PLoS ONE 6(9):e24096. doi:10.1371/journal.pone.0024096
42. Bechara C, Pallerla M, Zaltsman Y, Burlina F, Alves ID, Lequin O, Sagan S (2013) Tryptophan within basic peptide sequences triggers glycosaminoglycan-dependent endocytosis. Faseb J 27(2):738–749. doi:10.1096/fj.12-216176
43. Futaki S, Suzuki T, Ohashi W, Yagami T, Tanaka S, Ueda K, Sugiura Y (2001) Arginine-rich peptides. An abundant source of membrane-permeable peptides having potential as carriers for intracellular protein delivery. J Biol Chem 276(8):5836–5840. doi:10.1074/jbc.M007540200

Supplemental materials to

The stoichiometry of peptide-heparan sulfate binding as a determinant of uptake efficiency of cell-penetrating peptides

Rike Wallbrecher[1], Wouter P.R. Verdurmen[1], Samuel Schmidt[1], Petra H. Bovee-Geurts[1], Felix Bröcker[2,3], Anika Reinhardt[2,3], Toin H. van Kuppevelt[1], Peter H. Seeberger[2,3], Roland Brock[1]

[1]Department of Biochemistry, Nijmegen Centre for Molecular Life Sciences, Radboud University Nijmegen Medical Centre, Geert Grooteplein 28, 6525 GA Nijmegen, The Netherlands, Ph.: +31-24-3666213; Fax: +31-24-3616413

[2]Department of Biomolecular Systems, Max Planck Institute of Colloids and Interfaces, Arnimallee 22, 14195 Berlin, Germany

[3]Department of Chemistry and Biochemistry, Freie Universität Berlin, Arnimallee 22, 14195 Berlin, Germany

Corresponding email address: r.brock@ncmls.ru.nl

Table S1 Homology of the human lactoferrin-derived CPP with the corresponding amino acid sequences of lactoferrins of other mammalia.

origin	**sequence**
Human	KCFQWQRNMR-KVRGPPVSCIKR[1]
Chimpanzee	KCFRWQRNMR-RVRGPPVSCIKR
Dromedary	KCAQWQRRMK-KVRGPSVTCVKK
Horse	KCAKFQRNMK-KVRGPSVSCIKR
Goat	KCYQWQRRMR-KLGAPSITCVRR
Sheep	KCYQWQRRMR-KLGAPSITCVRR
Water buffalo	KCHRWQWRMK-KLGAPSITCVRR
Bovine	KCRRWQWRMK-KLGAPSITCVRR
Wild Yak	KCRRWQWRMK-KLGAPSITCVRR
Pig	KCRQWQSKIR-RTN-P-IFCIRR
Mouse	KCLRWQNEMR-KVGGPPLSCVKK
Rat	KCFMWQ-EMLNKAGVPKLRCARK

[1] Highly conserved residues are highlighted in underlined.

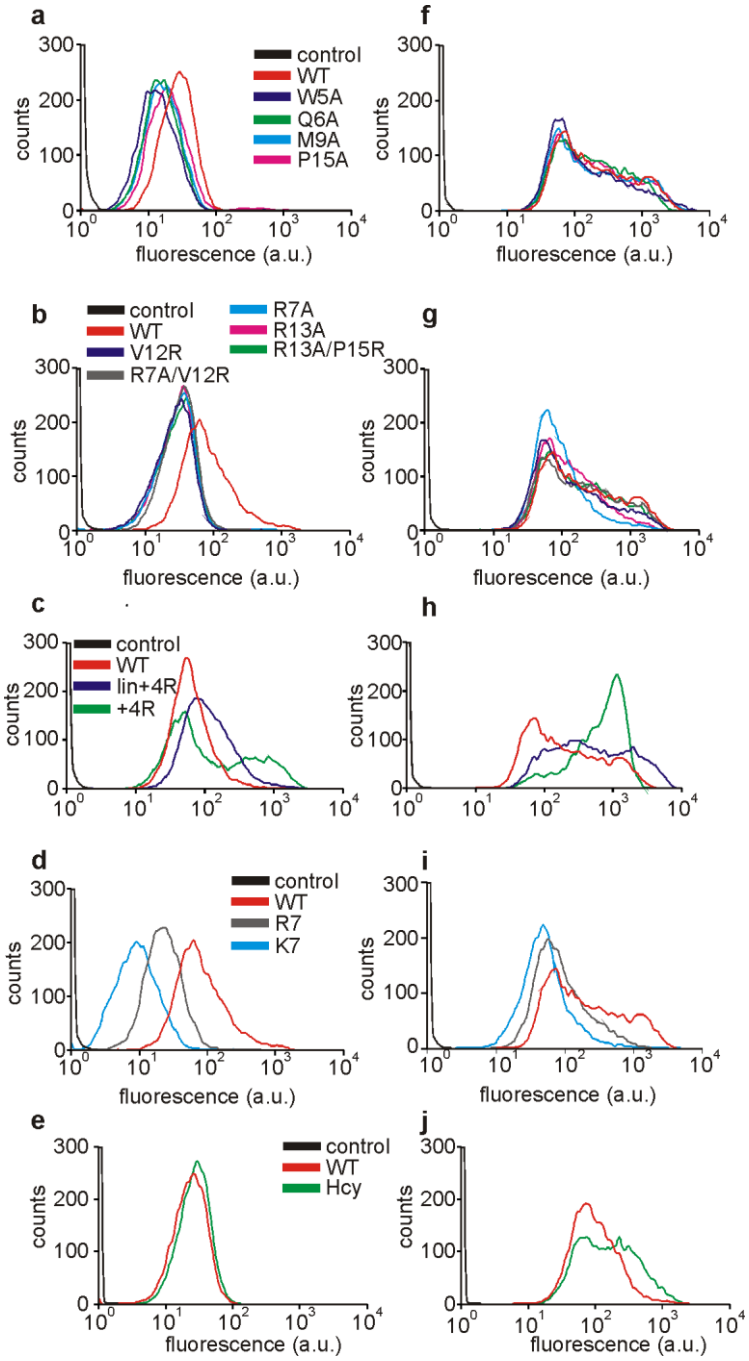

Fig. S1 Flow cytometry histograms of hLF variants in HeLa cells after a 30 min incubation at 37°C. (a-e) 5 µM, (f-j) 20 µM of the indicated peptides.

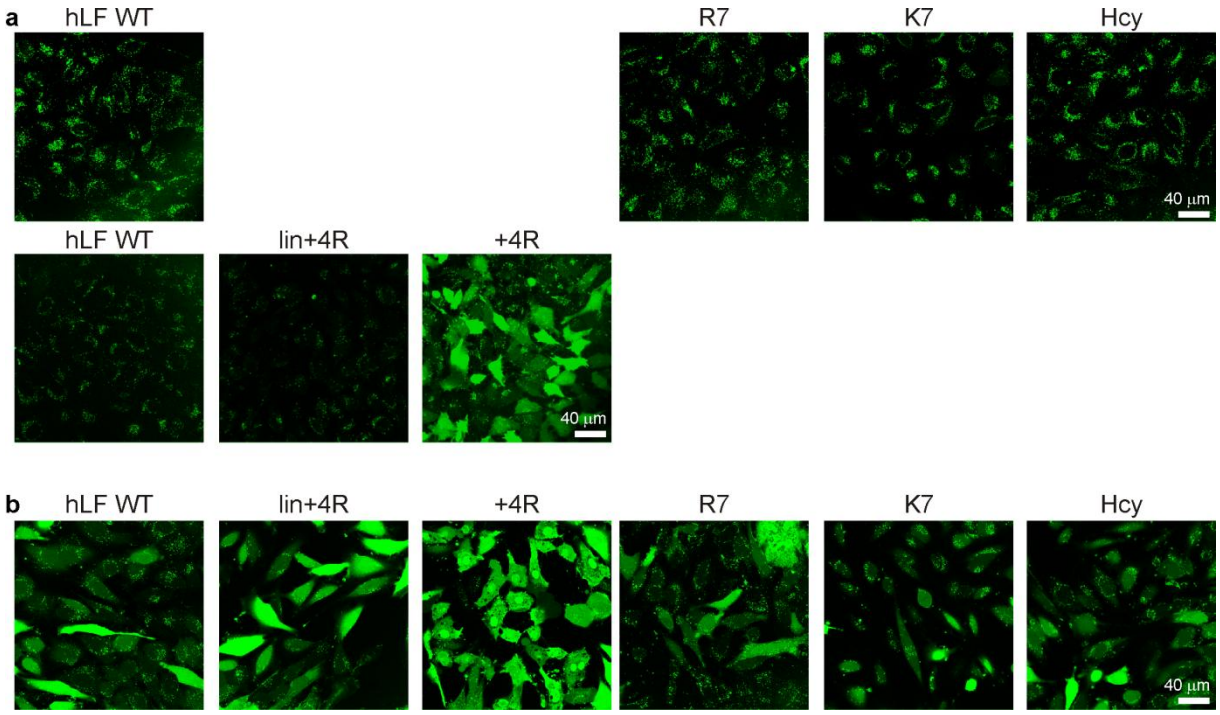

Fig. S2 Confocal microscopy of HeLa cells incubated for 30 min with 5 (a) or 20 µM (b) of the indicated peptides.

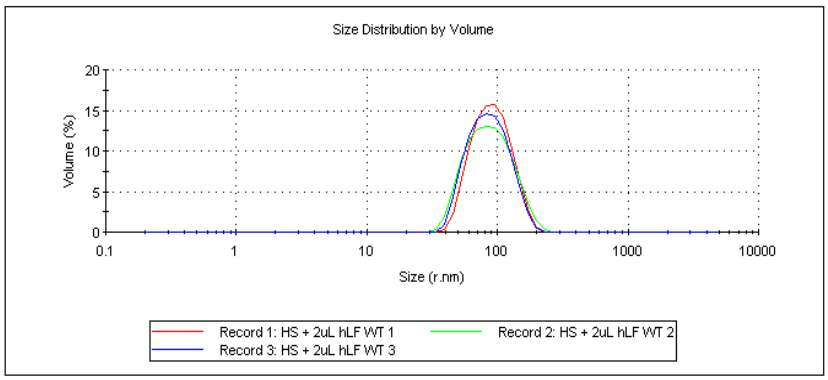

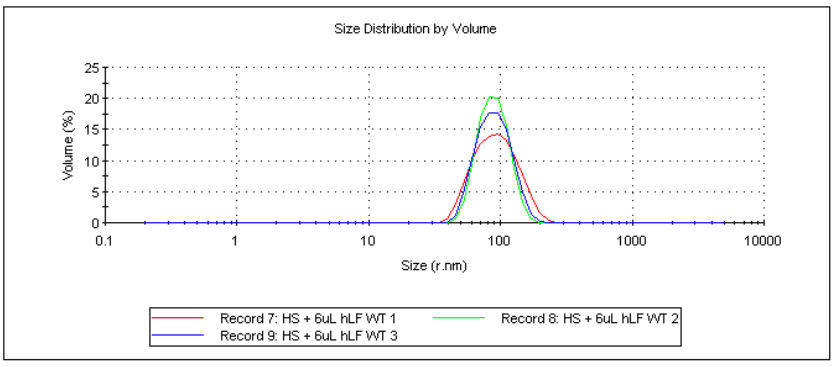

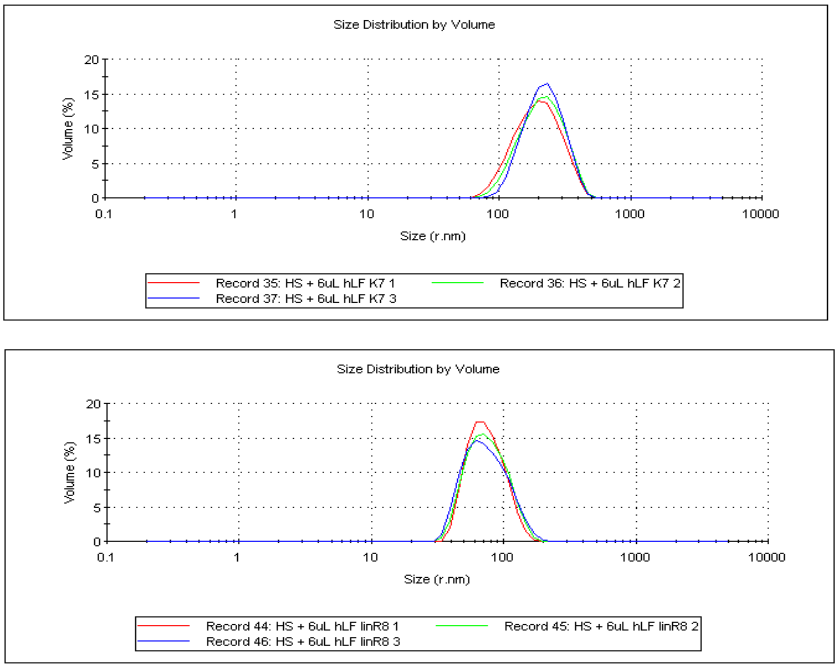

Fig. S3 Size distributions per volume of HS-peptide clusters determined by DLS. The different peptide solutions (50 µM) were titrated into 100 µL of a 10 µM HS solution in a ZEN0040 disposable cuvette. Samples were incubated for 3 min at 37 °C, were mixed again and 3x12 measurements were performed.

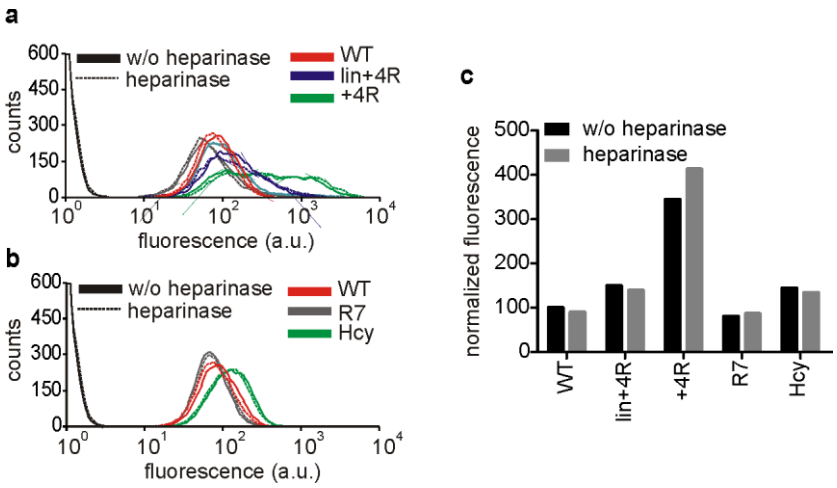

Fig. S4 Uptake of peptides at 5 µM after heparinase treatment. (a-b) Flow cytometry histograms, (c) normalized median fluorescence. One single experiment is shown.

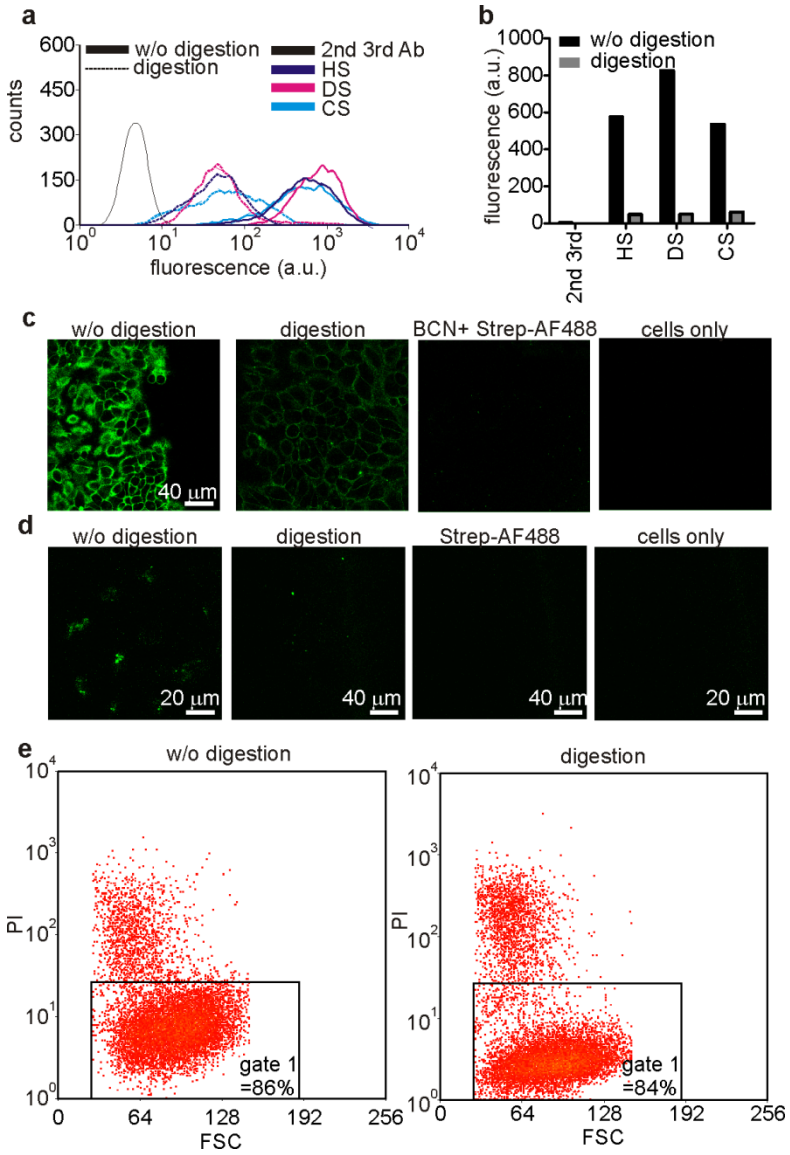

Fig. S5 Proof for efficient removal of the glycocalyx. After the incubation with the enzyme cocktail, HeLa cells were stained as described before [1] (a, b). Briefly, cells were incubated with single chain antibody fragments (scFv's) against epitopes of HS (HS4C3V-vsv), CS (I03H10V-vsv) and DS (LKN1V-vsv) for 45 min at RT. After washing with HBS, cells were incubated with the 2nd mouse-anti vsv (P5D4) antibody for 45 min at RT. Finally, cells were incubated with the 3rd antibody, goat-anti-mouse IgG Alexa Fluor 488) for 30 min at 4°C, detached by EDTA and measured by flow cytometry. (c) Staining of cell surface sialic acids was performed by metabolic labelling as described earlier [2]. Cells were incubated overnight in the presence or absence of 50 µM Ac4ManNAz. Cells were washed three times with HBS and incubated with 60 µM BCN-biotin (SynAffix, Nijmegen, the Netherlands) for 60 min at RT. After washing cells three times with HBS, and incubation with HBS containing Alexa Fluor 488-conjugated streptavidin (5 µg/mL) (Invitrogen, Eugene, USA) for 30 min at 4°C, followed by three final washing steps, cells were kept in pre-warmed culture medium and analyzed immediately by confocal microscopy. Detection of sialic acids by FACS was omitted because cell surface signal was lost already in non-digested metabolically labeled cells after detachment with EDTA. (d) A loss of the signal during detachments was observed for hyaluronic acid. Here, cells were incubated with biotin conjugated hyaluronic acid binding protein (HABP) (Sigma Aldrich, St. Louis, USA) for 45 min at RT, followed by Streptavidin-conjugated Alexa Fluor 488 incubation for 30 min at 4°C. Cells were kept in pre-warmed culture medium and analyzed by confocal microscopy. (e) Scatter plots showing the fraction of PI positive cells for the population of morphologically intact cells as gated by forward versus sideward scatter (not shown). Propidium iodide (2.5 µg/mL) was added to the cells directly before the measurement.

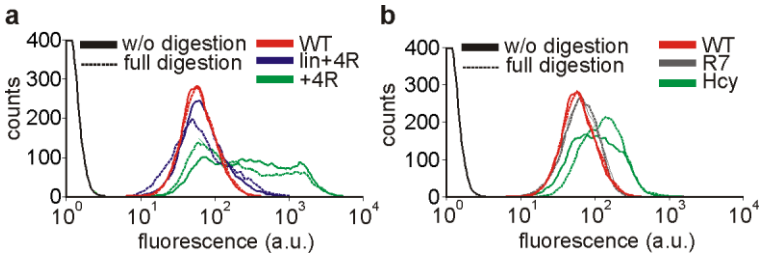

Fig. S6 Flow cytometry histograms of peptides after 30 min incubation at 37 °C at 5 µM after full digestion of the glycocalyx.

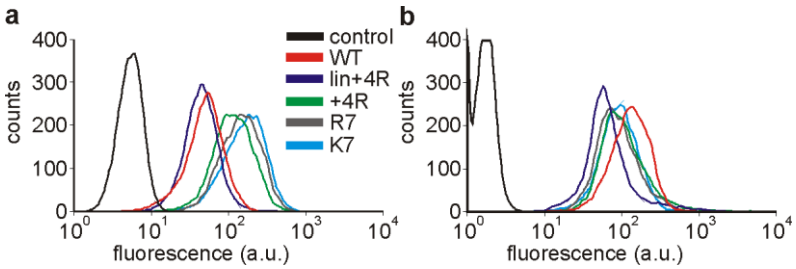

Fig. S7 Flow cytometry histograms of Jurkat cells incubated with 1 (A) and 5 µM (B) of the indicated peptides for 30 min at 37°C.

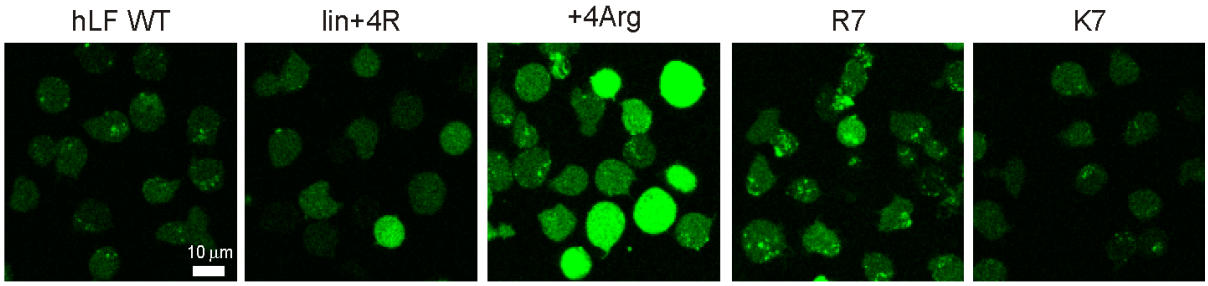

Fig. S8 Confocal microscopy of Jurkat cells incubated for 30 min with 5 µM of the peptides at 37°C.

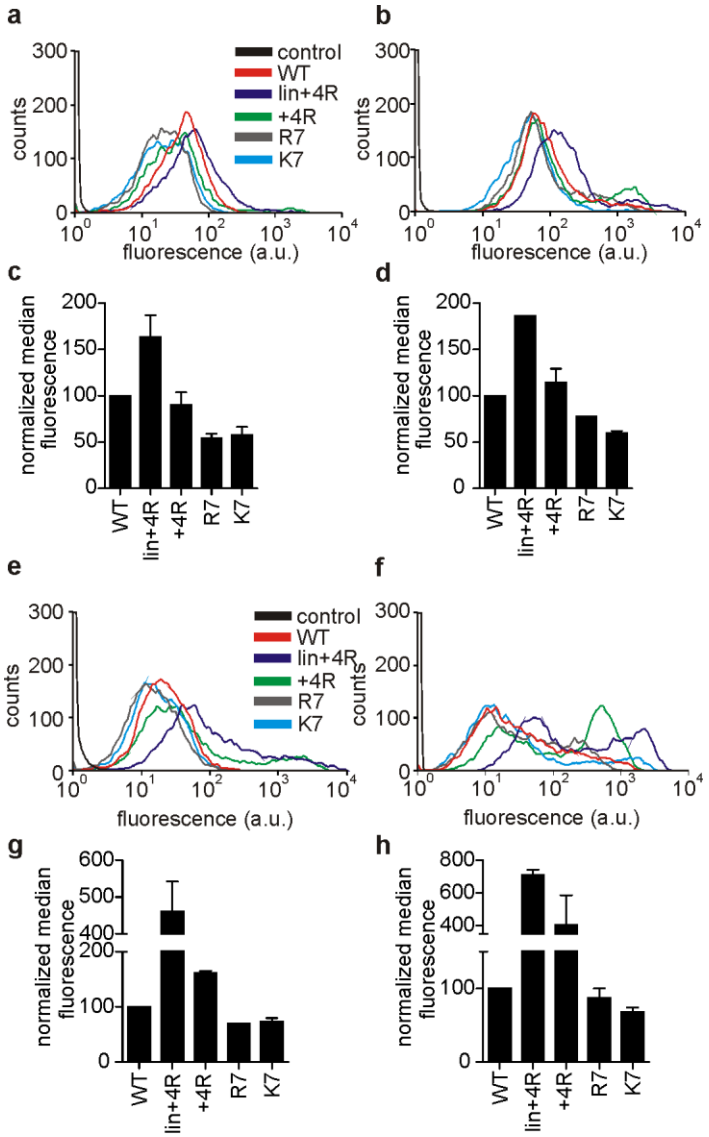

Fig. S9 Flow cytometry histograms and medians of Ovcar-3 cells incubated for 30 min at 37°C with 5 µM (a, c) or 20 µM (b, d) and Caco-2 cells at 5 µM (e, g) and 20 µM (f, h).

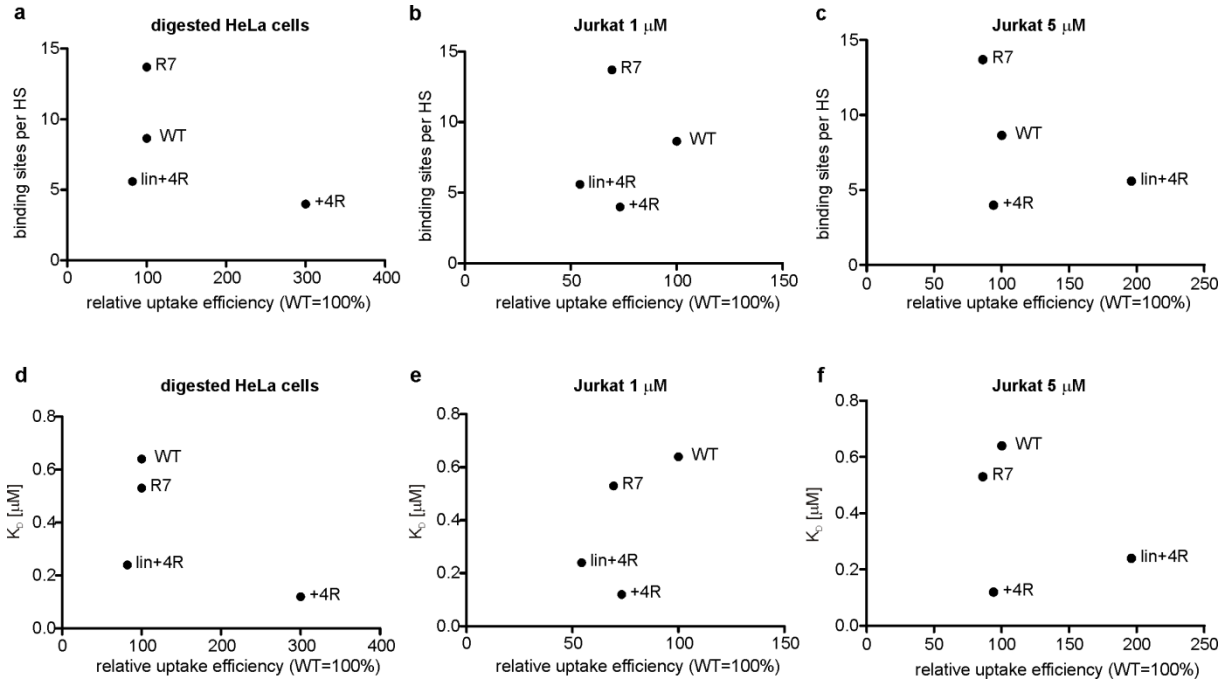

Fig. S10 Correlations between stoichiometry (a-c) and binding constant (d-f) with the uptake efficiency at 5 μM in digested HeLa cells or in Jurkat cells at 1 or 5 μM. Each point represents the mean of at least two experiments.

References

1. Verdurmen WP, Wallbrecher R, Schmidt S, Eilander J, Bovee-Geurts P, Fanghanel S, Burck J, Wadhwani P, Ulrich AS, Brock R (2013) Cell surface clustering of heparan sulfate proteoglycans by amphipathic cell-penetrating peptides does not contribute to uptake. J Control Release 170 (1):83-91. doi:10.1016/j.jconrel.2013.05.001

2. Dommerholt J, Schmidt S, Temming R, Hendriks LJ, Rutjes FP, van Hest JC, Lefeber DJ, Friedl P, van Delft FL (2010) Readily accessible bicyclononynes for bioorthogonal labeling and three-dimensional imaging of living cells. Angewandte Chemie 49 (49):9422-9425. doi:10.1002/anie.201003761